Eur. J. Mech. B/Fluids, **17**, n° 4, 571–586, 1998

Three-dimensional instabilities in wake transition

T. LEWEKE [a]*, C. H. K. WILLIAMSON [b]

ABSTRACT. – It is now well-known that the wake transition regime for a circular cylinder involves two modes of small-scale three-dimensional instability, modes "A" and "B", occurring in different Reynolds number ranges. These modes are quite distinct in spanwise lengthscale and in symmetry, and they are found to scale on different physical features of the flow.

Mode A has a large spanwise wavelength of around 3-4 cylinder diameters, and scales on the larger physical structure in the flow, namely the core of the primary Kármán vortices. The feedback from one vortex to the next gives an out-of-phase streamwise vortex pattern for this mode. In contrast, the mode B instability has a distinctly smaller spanwise wevelength (1 diameter) which scales on the smaller physical structure in the flow, namely the braid shear layer. The symmetry of mode B is determined by the reverse flow behind the bluff cylinder, leading to a system of streamwise vortices which are in phase between successive half cycles. The symmetries of both modes are the same as the ones found in the vortex system evolving from perturbed plane wakes studied by Meiburg and Lasheras (1988) and Lasheras and Meiburg (1990).

Furthermore, the question of the physical origin of these three-dimensional instabilities is addressed. We present evidence that they are linked to general instability mechanisms found in two-dimensional linear flows. In particular, mode A seems to be a result of an elliptic instability of the near-wake vortex cores; predictions based on elliptic instability theory concerning the initial perturbation shape and the spanwise wevelength are in good agreement with experimental observations. For the mode B instability, it is suggested that it is a manifestation of a hyperbolic instability of the stagnation point flow found in the braid shear layer linking the primary vortices. © Elsevier, Paris

1. Introduction

The wake of a circular cylinder, placed in a uniform flow perpendicular to its axis, is a classic example of an external open flow. The transition to turbulence in this system, as the Reynolds number is increased, has been studied for many years (*see*, e.g., the recent review by Williamson (1996a)). The Reynolds number, Re, is defined as $\mathrm{Re} = UD/\nu$, where U is the free-stream velocity, D the cylinder diameter, and ν the kinematic viscosity of the fluid. One important step on the route to turbulence is the instability of the stationary flow at Re = 47. It leads to a time-dependent wake structure, which is characterised by a periodic shedding of opposite-signed vortices, known as the Kármán vortex street. With suitable end conditions, the vortices are shed parallel to the cylinder and the periodic wake is two-dimensional.

Wake transition begins at a Reynolds number of about 190 and leads to a three-dimensional flow and a much less ordered state of vortex shedding. Some three-dimensional features of the flow at these Reynolds numbers were originally discovered as a spanwise waviness of the primary vortices, in the brief but significant observations of Hama (1957), as well as the growth of the waviness into "fingers of dye" by Gerrard (1978). It was shown experimentally in Williamson (1988) that the flow regime after this secondary instability involves a sequence of *two* modes of shedding, now generally referred to as modes A and B, with different spanwise length scales. The transitions to and between these modes, when increasing the Reynolds number, are accompanied by discontinuities in the dominant frequency of the vortex street wake. These observations were made possible by

[a] Institut de Recherche sur les Phénomènes Hors Équilibre, CNRS/Universités Aix-Marseille I et II, 12, avenue Général Leclerc, 13003 Marseille, France

[b] Sibley School of Mechanical & Aerospace Engineering, 252 Upson Hall, Cornell University, Ithaca, NY 14853-7501, USA

* Correspondence and reprints

0997-7546/98/04/© Elsevier, Paris

the control and elimination of large-scale three-dimensionalities, due to end effects, in the periodic regime, whose existence had made previous interpretations of experimental results somewhat ambiguous. Similar observations have since been made in other experimental studies (Mansy *et al.*, 1994; Zhang *et al.*, 1995; Brede *et al.*, 1996), and numerical studies (Zhang *et al.*, 1995; Thompson *et al.*, 1996; Mittal and Balanchandar, 1995; Persillon and Braza, 1998). In addition, recent numerical stability analyses (Noack and Eckelmann, 1994; Barkley and Henderson, 1996) have given information about the *linear* onset of the instability, whereas most experimental studies analyse the *non-linear* asymptotic flow state.

Despite the large number of recent investigations of this transition regime, the precise physical origin of the secondary instabilities of two-dimensional vortex shedding is still not clearly understood. Several mechanisms have been proposed. Leweke and Provansal (1995) used a Ginzburg-Landau equation to model the wake as a set of coupled oscillators. Based on the good agreement with experiments concerning the dynamics of the wake, they associated the transition to a Benjamin-Feir type instability found in such systems of oscillators. A drawback of this idea is the fact that the Benjamin-Feir instability has a vanishing spanwise wave number at the onset, whereas experimental and numerical observations show that the secondary mode A instability starts with a finite wavelength of about four cylinder diameters (Barkley and Henderson, 1996; Williamson, 1996b). Brede *et al.* (1996) considered the strongly curved streamlines in the near wake and suggested a centrifugal instability of the two-dimensional base flow, and in particular of the braid region between the primary vortices, as the mechanisms for transition to mode A. However, no conclusive evidence in support of this conjecture was presented. Karniadakis and Triantafyllou (1992) have proposed a period-doubling scenario for the wake transition, based on direct numerical simulations, although the recent work by Thompson *et al.* (1996) has shown that this behavior is possibly due to the small spanwise extent of their computational domain. Finally, Williamson (1996b) recently considered an instability mechanism found in elliptical flow (*see*, e.g., Landman and Saffman, 1987; Waleffe, 1990), which would lead to a three-dimensional deformation of the cores of the wake vortices, and therefore initiate the transition to the observed irregular vortex shedding.

In this paper, we further explore the physical origin of the two modes of three-dimensional instability observed in the wake of a circular cylinder, and their relation to more general mechanisms of instability. After a presentation of the transition modes A and B in section 2, including a discussion of their symmetry properties, we analyse in section 3 results from direct numerical simulations performed by H. Persillon (private communication, 1996) to identify the principal physical features of the two-dimensional wake flow which becomes unstable. We demonstrate the existence of regions with pronounced elliptic and hyperbolic flow in the primary vortex cores and braid shear layers respectively, which are known to be three-dimensionally unstable. In sections 4 and 5 we compare predictions from the theories of elliptic and hyperbolic instabilities with experimental observations in the cylinder wake concerning the transition mode A and B. The conclusions follow in section 6.

2. Instability modes A and B

In this section, we recall the characteristic features of the transition modes in the circular cylinder wake, as observed in experiments. The transition regime for this flow is found in a Reynolds number range 190-260 approximately. The existence of two different modes (A and B) of three-dimensional vortex shedding in this regime was briefly presented by Williamson (1988) and more comprehensively in Williamson (1996b), where additional details and information on the experimental techniques can be found.

Figure 1 shows dye visualisations of the near wake behind the cylinder, showing the vortex street structure for both modes in planview. In mode A (*Fig.* 1a), the primary vortices deform in a wavy fashion along their length. The spanwise wavelength λ_A of these perturbations is a slowly decreasing function of Reynolds number and varie between 4 and 3 cylinder diameters. The photograph in Figure 1a was taken in the early stages of a towing

tank experiment, where the cylinder was started from rest, at a time when mode A exists in a relatively pure form. As the flow progresses, the waviness grows from one cycle to the next, resulting in the local spanwise formation of vortex loops, which become stretched into streamwise vortex pairs in the braid regions between the primary vortices. Mode A is clearly evident in the range $190 < \mathrm{Re} < 240$.

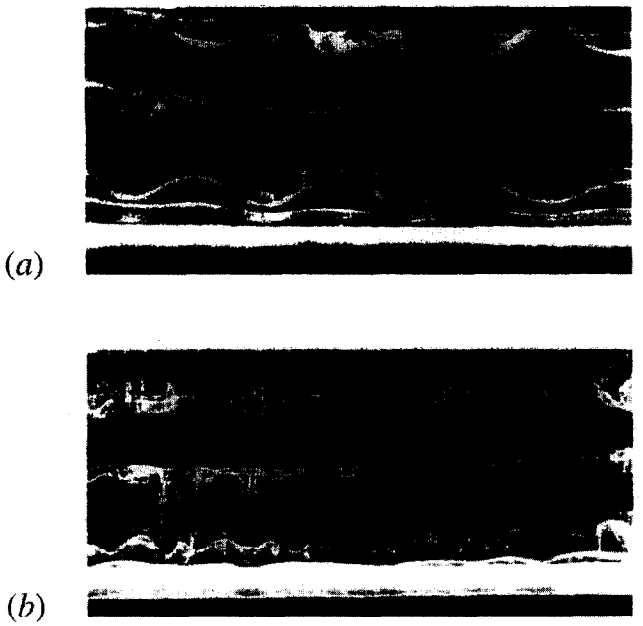

Fig. 1. – Visualisations of the three-dimensional instability modes A and B in planview, flow is upward. The photographs are to the same scale. (*a*) Mode A at Re = 200, associated with a spanwise waviness of the Kármán vortices with wavelength $\lambda/D = 4$. (*b*) Mode B at Re = 270, associated with the inception of small-scale streamwise vortex pairs at a spanwise wavelength $\lambda/D = 1$.

At higher Reynolds numbers, around and above Re = 240, a different kind of vortex shedding, the transition mode B, is observed, as shown in Figure 1b to the same scale as Figure 1a. The primary vortices are much more uniform in the spanwise direction than for mode A, but fine-scale streamwise vortex pairs are now formed, at a significantly smaller spanwise wavelength λ_B of about one cylinder diameter. This wavelength varies little with Reynolds number.

The marked disparity in spanwise wavelength and visual appearance between modes A and B suggests that they are due to two different instabilities of the two-dimensional vortex street flow. Before exploring this idea in more detail, however, we take a look at the symmetry properties associated with the two transition modes.

As explained in Williamson (1996b), the wavy perturbation of a primary vortex in mode A carries over from one vortex to the next one, shed in the following half cycle from the opposite side of the cylinder. Since this next vortex has an opposite-signed vorticity, it is natural to expect an *out-of-phase* streamwise vorticity pattern between successive half cycles of shedding. Figure 2 shows images from video sequences of visualisations in a plane located in the near wake perpendicular to the free stream. The passage of fluorescent dye (washed off the body) through the light sheet, shows the distinct symmetries of the streamwise vortices. Figure 2a corresponds to mode A and was made in similar conditions as in Figure 1a, except that the cylinder was fixed and the flow (in a water channel) started gradually from rest. The dye pattern in the second photograph of Figure 2a is a mirror image of the first, taken half a shedding cycle earlier, showing the out-of-phase symmetry of the streamwise vorticity.

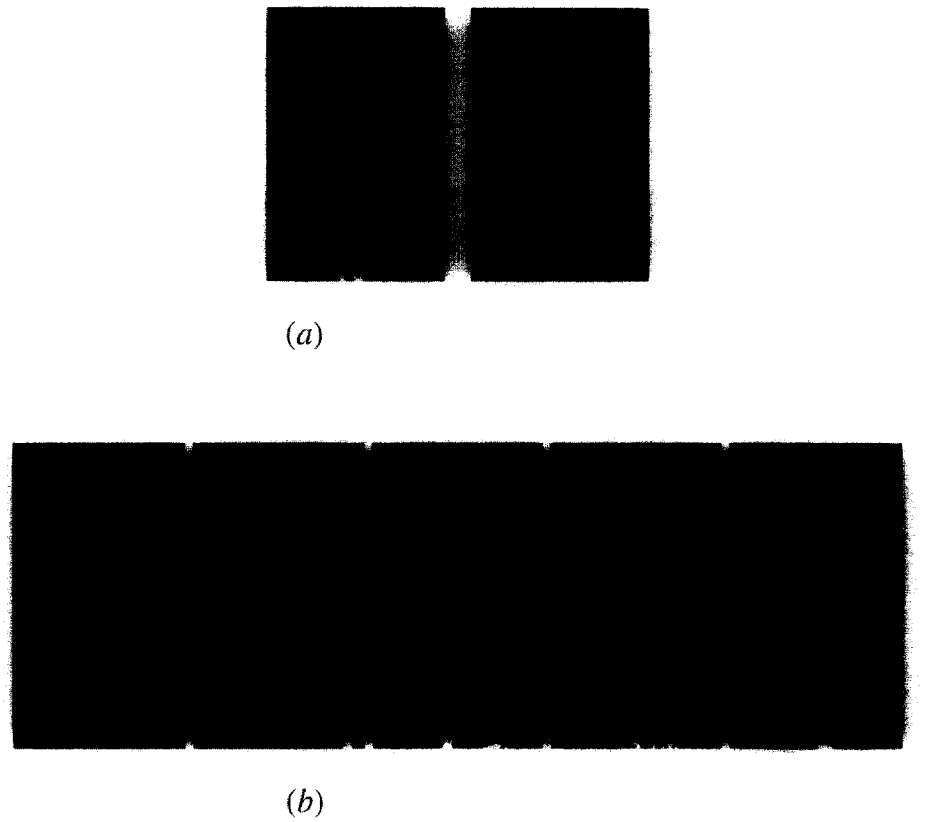

Fig. 2. – Visualisations of the streamwise vortex pattern in a plane perpendicular to the free stream, approximately two diameters behind the cylinder, which extends vertically in this figure. (*a*) Mode A at Re = 190. The images, separated by 1/2 shedding cycle, clearly show the out-of-phase symmetry of mode A. (*b*) Mode B at Re = 280. The sequence covers half a shedding period and demonstrates the in-phase symmetry of this mode between half-cycles of vortex shedding.

For mode B, the symmetry of the small-scale streamwise vortices is linked to the existence of a reversed-flow region behind the bluff body. These secondary vortices develop in the shear layers which separate from each side of the cylinder, and which subsequently form the vorticity "braids" linking consecutive primary vortices (*see* section 3 below). The reverse flow in the near wake has the effect of bringing the perturbed shear layer, formed earlier on one side of the body, back upstream in the vicinity of the freshly emerging shear layer on the other side of the body. This imprints an initial perturbation on the latter which is *in-phase* with the one of the former, and which is then rapidly amplified into a new set of streamwise vortices by the strain experienced by the shear layer. This process is illustrated in the visualisation sequences of Figure 2b, which is shown to the same scale as Figure 2a and also covers half a shedding period. The first image shows the very regular array of counterrotating streamwise vortices, which were generated in the separating (braid) shear layer, during the time a (vertically-oriented) primary vortex formed and shed from the left side of the near wake, as one looks upstream. During the growth and subsequent shedding of a right-side primary vortex, the streamwise vortices are rapidly convected across the wake of the right side, where they seem to amalgamate with the newly forming secondary vortices of the right shear layer. Except for some minor vertical (spanwise) shifts, the patterns in the first and last image are identical: the streamwise vortices are in phase between half cycles for mode B.

For clarity, Figure 3 summarizes schematically the vorticity configurations of modes A and B, illustrating the different symmetries of the wake transition modes.

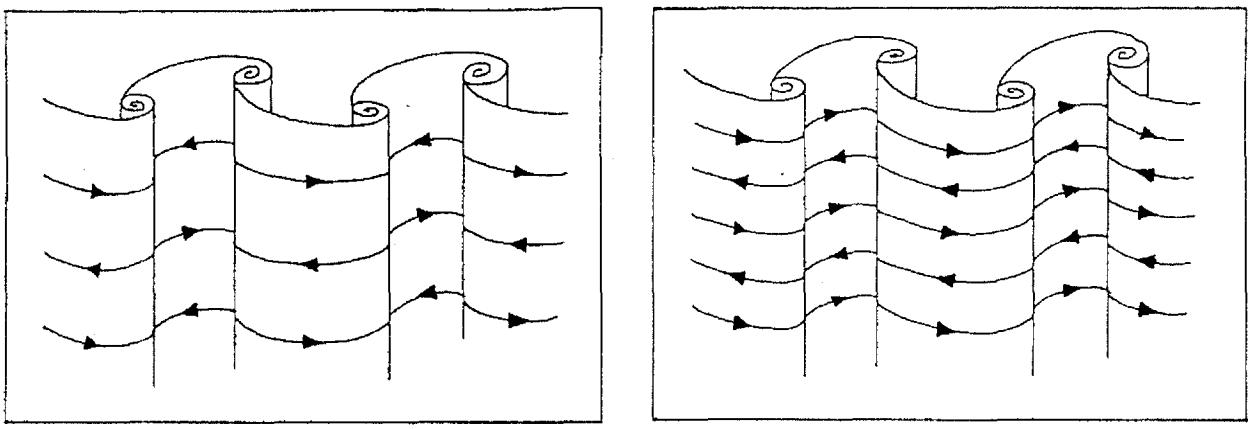

(a) (b)

Fig. 3. – Symmetry diagrams of the three-dimensional modes. (*a*) Mode A, of large spanwise wavelength, with its out-of-phase sequence of streamwise vortices from one braid to the next. (*b*) Mode B, of smaller spanwise wavelength, comprises an in-phase arrangement.

The results presented in this section, concerning the overall features, the wavelengths, and the symmetries of two modes of the transition regime are consistent with several observations made in other recent experimental, numerical, and theoretical studies, which are reviewed in Williamson (1996a). In particular, Brede *et al.* (1996) propose, based on time sequence of (DPIV) velocity measurements in a plane similar to the one visualised in Figure 2, that the streamwise vortices of mode B make up 'continuous vortex tubes' running from side to side between the primary vortices. The apparent amalgamation of successive sets of streamwise vortices observed in Figure 2b would explain how the streamwise vortex tubes might appear as 'continuous', as interpreted by Brede *et al.* (1996).

Although the existence of *two* distinct three-dimensional modes in the bluff-body wake has been known for some time (Williamson, 1988), it was only very recently that their symmetries were deduced from experimental evidence. However, Meiburg and Lasheras (1988; *see* also Lasheras and Meiburg, 1990) have demonstrated, both experimentally and numerically, the existence of two distinct three-dimensional vorticity modes, when a plane wake flow (as occurs downstream of a splitter plate) is perturbed. These are shown here for clarity in Figure 4. By indenting the splitter plate, their "mode 2", or "symmetric" mode, in Figure 4a, has the same symmetry as the mode A found for bluff bodies. By using a corrugated plate, they were able to observe a "mode 1" or "non-symmetric" mode, in Figure 4b, which has the same symmetry as the bluff-body mode B instability. The existence of such mode symmetries in a general wake flow was thus shown clearly in these studies. Ongoing work by Julien, Lasheras and Chomaz (1997) indicates that both modes 1 and 2, with roughly the same wavelength, can occur under unperturbed conditions. In fact, it can be shown, using the spatio-temporal symmetries of the Kármán vortex street base flow, that any small perturbation of this flow, satisfying the linearised Navier-Stoke equations governing its evolution, must be either symmetric or antisymmetric.

Concerning the unforced wake of a circular cylinder under consideration here, the above general results imply that *if* a three-dimensional instability exists, the corresponding perturbation should have one of these two symmetries, which is indeed the case. However, these above related results do not predict the existence of two distinct instabilities. Nor are the symmetries of the modes known *a priori*. The two instabilities, their symmetries and the physical mechanisms at the origin of the instabilities are addressed in Williamson (1996b) and in the present paper.

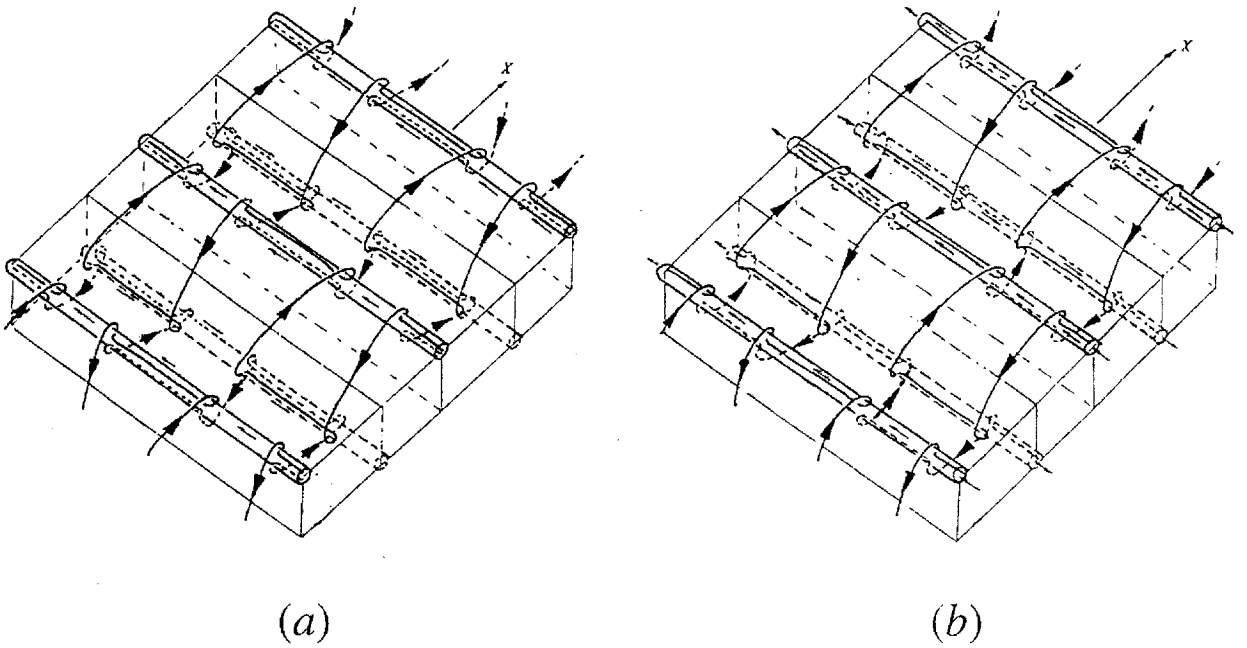

Fig. 4. – Diagrams of the three-dimensional vortex patterns observed in perturbed plane wakes by Meiburg and Lasheras (1988, modified *Figs.* 22 and 15, with permission). (*a*) "Mode 2" with out-of-phase symmetry of streamwise (X-direction) vorticity. (*b*) "Mode 1" with in-phase symmetry of streamwise vorticity.

3. Properties of the two-dimensional wake

This section is devoted to a closer analysis of the *two-dimensional* wake flow in the transition regime. The three-dimensional instabilities of this base flow lead to the vortex shedding modes A and B. The results presented in this section were obtained using the velocity data from a two-dimensional direct numerical simulation (DNS) carried out by H. Persillon (private communication, 1996) and kindly made available to the authors. The Reynolds number is these calculations was Re = 100, *i.e.* slightly above the onset of wake transition. Details about the numerical procedure can be found in Persillon and Braza (1998).

Figure 5 shows the principal features of the two-dimensional cylinder wake for Reynolds numbers in the transition regime. In Figure 5a, contours of the instantaneous spanwise vorticity at one instant in the shedding cycle are given. The main characteristics of the flow that can be identified from this distribution are presented in Figure 5b. The boundary layer separating from the lower side of the cylinder is seen to roll up into a new primary vortex about $1D$ behind the body. The vortex to the right of it has rolled up from the upper shear layer half a shedding cycle earlier. Part of the layer is still trailing behind this vortex, forming the so-called braid between consecutive vortices. In this paper, the free shear layers separating from the body or apparently running between primary vortices, as the wake convects downstream, are both termed "braid shear layer".

The two main features of the two-dimensional near wake are the rolled-up primary vortices and the braid shear layers. As seen in Figure 5b, two different length scales are associated with these structures. The cores have a diameter $\delta_{\mathrm{core}} \approx D$, whereas the shear layer (vorticity) thickness is $\delta_{\mathrm{braid}} \approx D/4$. The ratio $\delta_{\mathrm{core}}/\delta_{\mathrm{braid}}$ is surprinsingly close to the ratio $\lambda_{\mathrm{A}}/\lambda_{\mathrm{B}}$ of the spanwise wavelengths of the transition modes A and B. This suggests that there may be a connection between the two wake features and the three-dimensional instabilities leading to these two modes.

It was proposed in Williamson (1996b) that the mode A instability with the larger spanwise wavelength is linked to the larger flow structure in the wake, *i.e.* the vortex cores, and that it is due to an elliptic instability of these cores. This mechanism acts in two-dimensional flows with elliptical streamlines, which are a superposition of a constant-vorticity rotation and a plain strain. Three-dimensional instability occurs through a resonant amplification of inertial waves. Elliptic instability has been treated theoretically by Pierrehumbert (1986), Bayly (1986), Landman and Saffman (1987), Waleffe (1990), Lifschitz and Hameiri (1991), and a number of others more recently. In order to demonstrate the link between elliptic flow and the cylinder wake, it is useful to look at the flow field inside a primary vortex in a frame of reference moving with that vortex. This is shown in Figure 6 for the lower vortex of Figure 5, which is convected downstream (at this point in time) at a speed of about one half the free-stream velocity U. In the core of this vortex, the streamlines are indeed approximately ellipses, with an aspect ratio of about 2. In an ideal elliptic flow (*see* Equation (1) below), the principal stretching axis of the brain is inclined 45° with respect to the major axis of the elliptic streamlines. Calculations made for the flow field typified by Figure 6 show very clearly that both vortices have this property (Williamson, 1996b).

Figure 6 also gives information about the type of flow in the upper braid shear layer, which, at the particular instant depicted in Figures 5 and 6, is moving at the same speed as the lower vortex core. Figure 6 reveals the

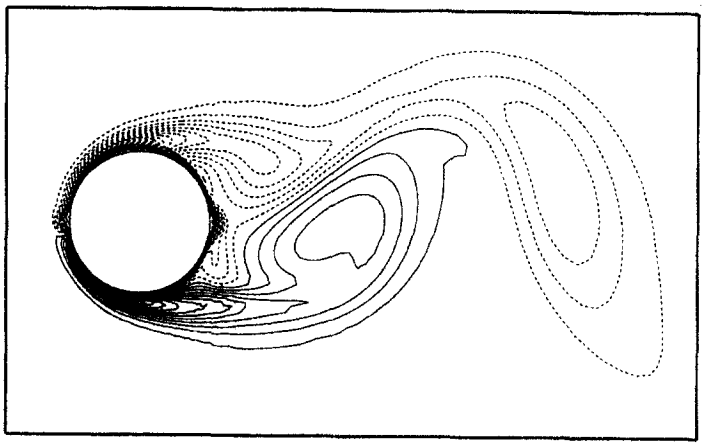

(*a*)

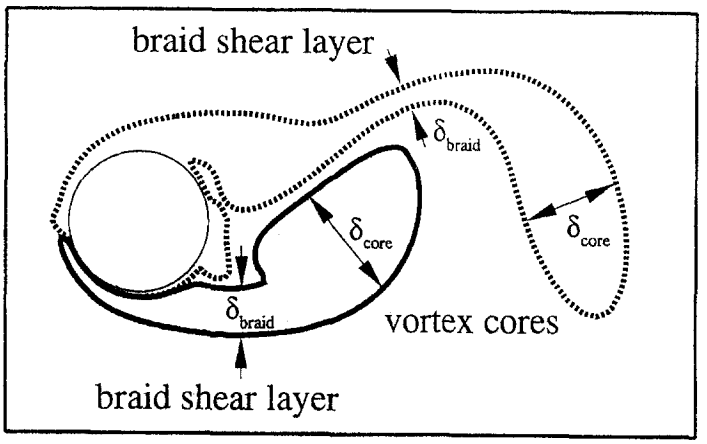

(*b*)

Fig. 5. – Spanwise vorticity ω of the two-dimensional wake flow at Re = 200, from direct numerical simulations by Persillon and Braza (private communication, 1996). (*a*) Contours of vorticity at levels $(\omega D/U) = \pm 0.5, \pm 1.5, \pm 2.5$, etc. (*b*) Sketch of the principal physical flow features.

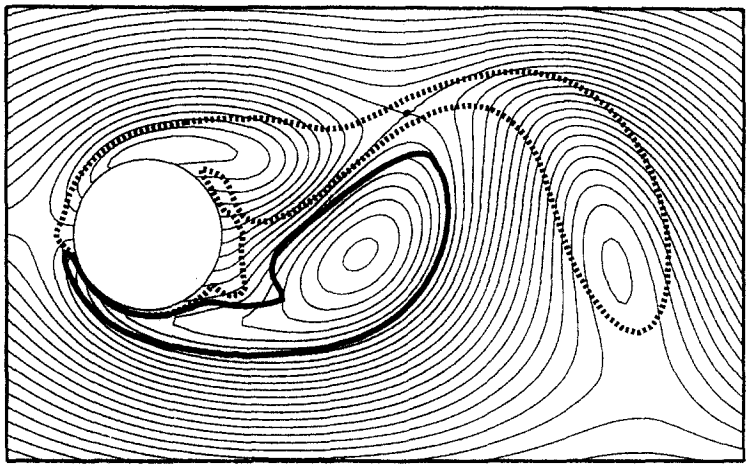

Fig. 6. – Streamlines of the flow in Figure 5, in a frame of reference moving with the lower vortex, *i.e.* at approximately $U/2$ in the downstream direction. This plot shows the elliptic shape of the streamlines in the vortex core, as well as the stagnation point flow in the braid shear layer.

presence of a stagnation-point, or hyperbolic, flow in the braid shear layer. Hyperbolic flow is another kind of linear flow resulting from a superposition of rotation and plain strain, but contrary to elliptic flow, the strain dominates over the rotation. The limit between the two types is plane Couette flow.

Two-dimensional flows which depend linearly on the spatial coordinate x and y can be expressed in the form

$$\mathbf{V} = \begin{pmatrix} 0 & -\frac{\omega}{2} - \varepsilon \\ \frac{\omega}{2} - \varepsilon & 0 \end{pmatrix} \begin{pmatrix} x \\ y \end{pmatrix}, \tag{1}$$

where ω and $\varepsilon > 0$ are the vorticity and strain rate, respectively. Without loss of generality, the direction of maximum stretching of the strain is at an angle of –45° to the horizontal. The flow is elliptic for $\varepsilon < |\omega|/2$, and hyperbolic for $\varepsilon > |\omega|/2$. In the former case, the quantity $\beta = 2\varepsilon/|\omega|$ represents the eccentricity of the elliptic streamlines, but it will be used in the following to characterise any kind of linear flow.

It has been shown by different authors, cited earlier, that unbounded flows of the form (1) are three-dimensionally unstable for all values of β, except $\beta = 1$; plane Couette flow is marginally stable. Concerning the results for hyberbolic flow, *see* e.g. Lagnado *et al.* (1984) and Lifschitz and Hameiri (1991). For inviscid flow, the growth rate σ_i of the most untable perturbations are given by

$$\frac{\sigma_i}{\varepsilon} = \begin{cases} f(\beta) \approx \dfrac{9}{16}(1 - \beta^m)^n & \text{for} \quad 0 < \beta < 1 \text{ (elliptic flow)} \\ \sqrt{1 - \beta^{-2}} & \text{for} \quad \beta > 1 \text{ (hyperbolic flow)} \end{cases} \tag{2}$$

The approximate expression for the elliptic instability growth rate, with $m = 2.811$ and $n = 0.3914$, was computed here from a least-squares fit to the numerically determined result presented by Landman and Saffman (1987). The result for hyperbolic instability was given by Lagnado *et al.* (1984). The growth rate depends on the *orientation* of the perturbation wave vector, and, in an unbounded domain, not on its *magnitude*; perturbations at all wavelengths λ_z are equally unstable. In Figure 7, the results of Equation (2) are summarized in a single plot.

Although the growth rates of the three-dimensional instabilities were found for an unbounded, inviscid, and stationary flow, it may be instructive to calculate them locally for the two-dimensional and time-dependent cylinder wake in the transition regime. This is done in Figure 8, for elliptic and hyperbolic flow regions separately, always using the same DNS data as for Figures 5 and 6. For the elliptic instability, high values

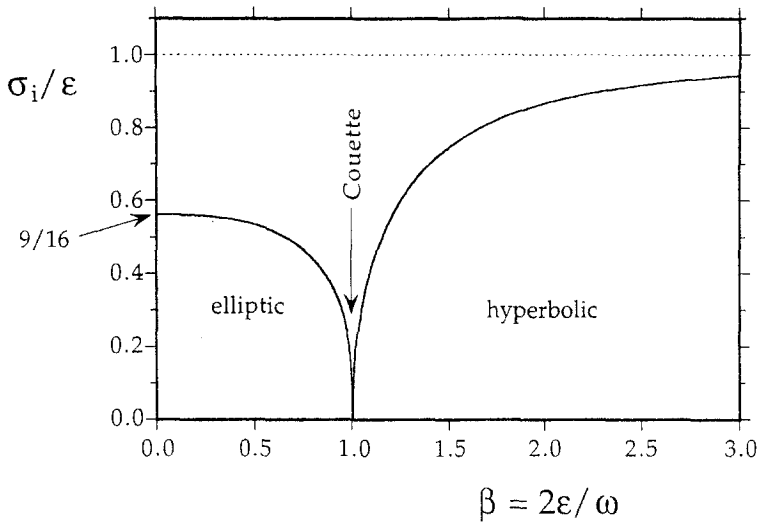

Fig. 7. – Growth rate of three-dimensional instabilities of two-dimensional inviscid linear flows, as function of the generalised eccentricity parameter β. Results deduced from Landman and Saffman (1987) and Lagnado *et al.* (1984).

of the locally calculated inviscid growth rate are found mainly in the primary vortex cores, whereas for the hyperbolic instability, high growth rates are localized in the braid shear layer between the primary structures. Figure 5a shows that the vorticity is approximately constant within these regions. The DNS results show a similar behaviour for the strain, and consequently for the eccentricity parameter β. It is also known from the studies by Waleffe (1990; *see* also section 4) and Leblanc and Godeferd (1998) that there exist localised modes of the elliptic and hyperbolic instabilities that would 'fit' into these regions and essentially 'see' a uniform elliptic or hyperbolic flow. It seems therefore legitimate to expect, from the results shown in Figure 8, the development of an elliptic instability in the primary vortex cores, and a hyperbolic instability in the braid shear layers. In addition, the stability analysis of Barkley and Henderson (1998) has shown that contours of perturbation velocity for mode A are largely concentrated in the spanwise vortex cores, while for mode B the concentration is stronger in the braid regions. This is clearly consistent with the present results of Figure 8. However, it must be stated that the results of Barkley and Henderson pertaining to this point in their Figure 11, are only "qualitative" as recently pointed out to the authors by Ron Henderson (private communication, June 1998). We suggest here that these two instability mechanisms are at the origin of the observed wake transition modes A and B.

After the qualitative arguments presented in this section, we put forward, in the next sections, a more quantitative comparison between theoretical predictions concerning these instabilities, and experimental observations. For this, we will also take into account the fact that the "real" (two-dimensional) wake flow is viscous and time-dependent, and that the regions of elliptic or hyperbolic flow are of finite extent.

4. Elliptic instability and mode A

In this section, we present evidence to support our suggestion that the inception of mode A vortex shedding behind a circular cylinder is due to an elliptic instability of the primary vortex cores in the near wake.

For a first qualitative comparison between elliptic instability theory and experimental observations, it is useful to visualize the spatial structure of the perturbation associated with this instability mechanism. As shown in Leweke and Williamson (1998) and Eloy and Le Dizès (1998), the most unstable perturbation in a finite-size region of elliptical flow, e.g. a vortex core, closely resembles the particular localised perturbation solutions given by Waleffe (1990) for unbounded elliptic flow (Equation (1)) in the limit of vanishing strain ε. This

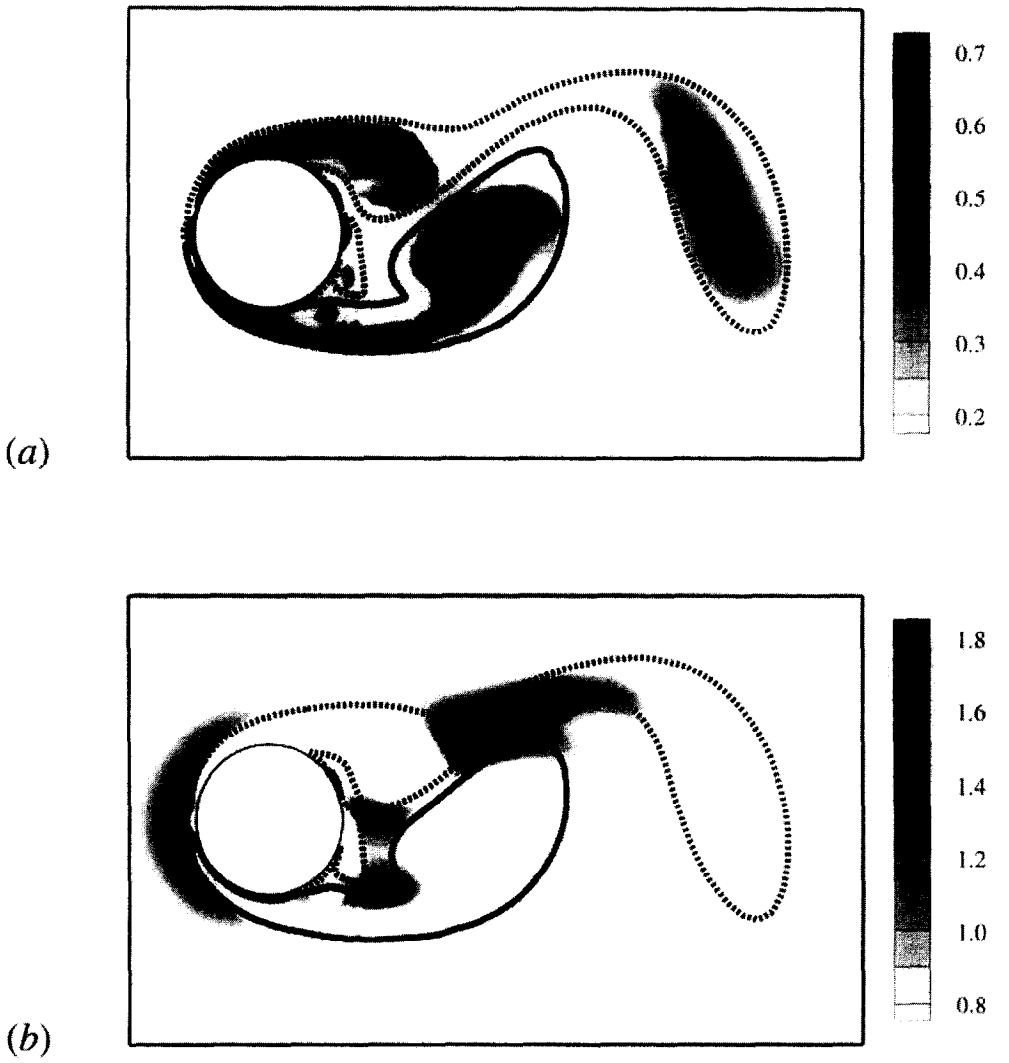

Fig. 8. – Regions of possible three-dimensional instability, as indicated by the inviscid growth rate $\sigma_i D/U$ (see *Fig.* 7), calculated locally from the distribution of β and ε in the two-dimensional flow. (*a*) Growth rate of elliptic instability for $0 < \beta < 1$ (*b*) Growth rate of hyperbolic instability for $\beta > 1$.

perturbation is shown in Figure 9b as a streamline plot in the x-y plane containing the two-dimensional base flow. When this perturbation, with its characteristic two-lobe structure, is added to the base flow in Figure 9a, one obtains a total flow, shown in Figure 9c, in which the center of rotation is displaced in the direction of maximum stretching of the strain, indicated by the dotted line. In addition, there exists an invariant streamline, which is unaffected by the perturbation, and layers inside and outside this line are displaced in opposite radial directions. The pattern in Figure 9c is modulated in the perpendicular axial direction. A longitudinal cut through the vortex in the stretching plane is given in Figure 10, showing the wavy displacement of the vortex center and the invariant stream tube. For low strain, the axial wavelength of the most unstable perturbation is almost exactly twice the diameter of this invariant tube.

This prediction, derived from theoretical considerations, can be compared to observations of the spatial structure of mode A. Figure 11 shows a visualization of the very initial stages of the mode A instability. The

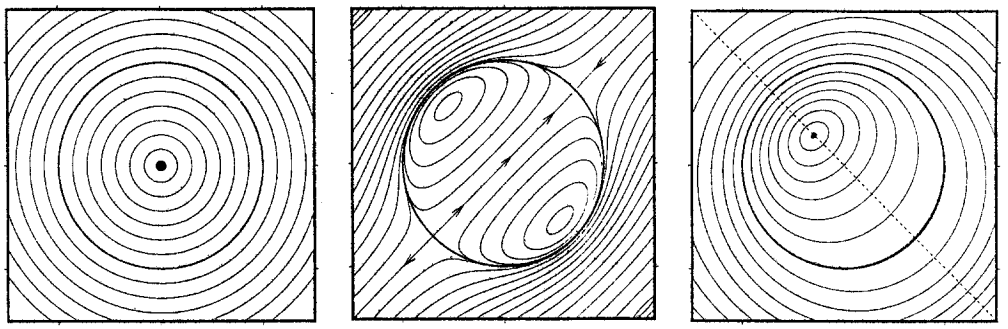

(a) (b) (c)

Fig. 9. – Streamlines associated with the most amplified elliptic instability mode in a finite-size region (e.g. vortex core), in the limit of vanishing strain in the –45° direction. (*a*) Base flow. (*b*) Perturbation (Waleffe, 1990). (*c*) Total flow. The perturbation displaces the centre of rotation in the stretching direction of the strain.

photograph was taken shortly after the start of the cylinder motion in a towing tank experiment, similar to the one for Figure 1, well before the localized vortex loops and dislocations appear. In this picture, the thick dye filament marking the center of a primary vortex, exhibits the same characteristic waviness as would be expected from elliptic instability. Not far from this filament, one can see a layer which does not seem to be disturbed in the spanwise direction, and which possibly corresponds to the invariant stream tube.

A more quantitative comparison can be made concerning the spanwise wavelength of the instability. As mentioned above, for small strains ε and nearly-circular flow, the axial length scale of the most unstable

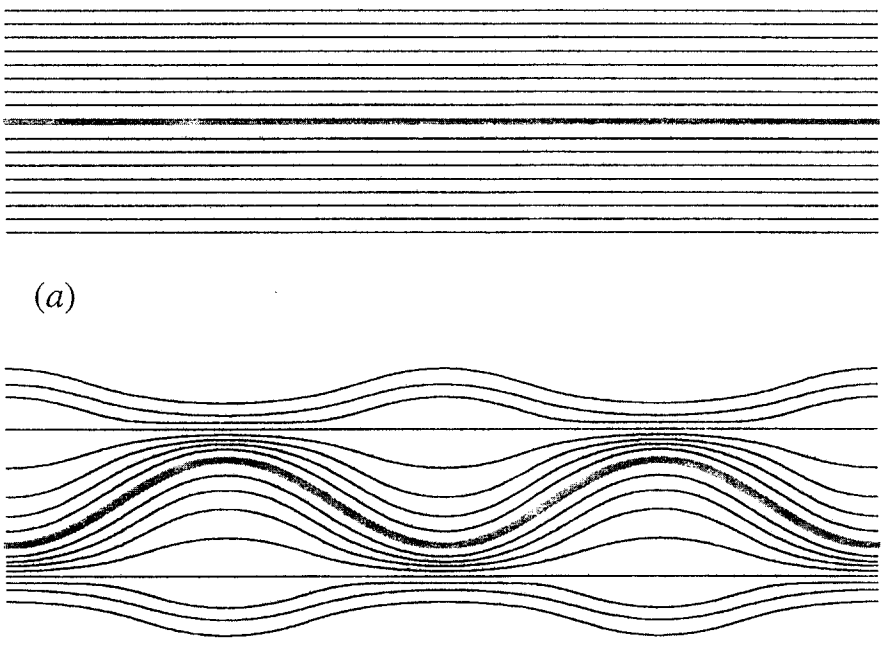

(a)

(b)

Fig. 10. – Longitudinal cut through stream surfaces of the (*a*) unperturbed and (*b*) perturbed vortex of Figure 9. The position of the cut is marked by the dashed line in Figure 9c.

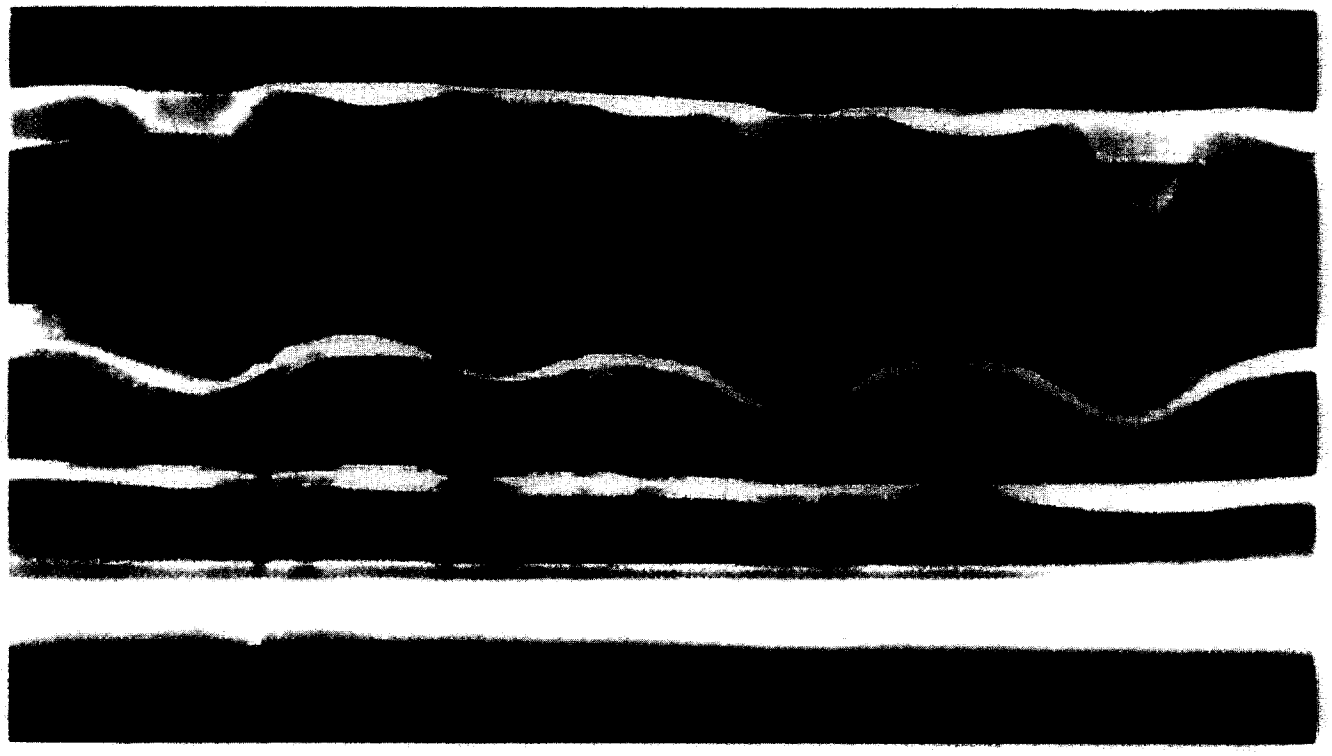

Fig. 11. – Dye visualisation of the near wake structure at Re = 200, the flow is upward. The photograph was taken approximately 8 shedding cycles after the start of the cylinder in a towing tank. It shows the characteristic wavy deformation of the vortex centre in the early stages of the mode A instability.

perturbations is linked to the length scale in the cross-sectional plane (diameter of the invariant streamline), which itself depends on the size of the elliptical region. However, the elliptic flow in the cores of the primary vortices in the cylinder wake does not have a low strain. From the DNS data, the streamline eccentricity is found to be relatively high: $\beta \approx 0.6$. Nevertheless, a similar relation between cross-sectional and axial length scales can be found for this case from the analysis of Landman and Saffman (1987):

$$\lambda = L\left(\frac{2}{1-\beta}\right)^{1/2} \tan\theta. \tag{3}$$

Here, λ is the axial wavelength, and θ the angle between the wave vector of the most unstable perturbation and the axis of rotation of the base flow. L represents the length scale of the perturbation in the cross-sectional plane. Because of viscous damping effects at small scales (*see* Equation (5) below), the most unstable perturbation is the one at the largest scale. This mean that L corresponds to the overall size of the region of elliptical flow, which, in our particular case, is given by the diameter of the primary cores δ_{core} (see *Fig.* 5b and 8a). From Figure 3 of Landmann and Saffman (1987) one obtains $\theta \approx 53^{\circ}$ for $\beta = 0.6$. Together with $L = \delta_{\mathrm{core}} \approx D$, this leads to

$$\lambda \approx 3D. \tag{4}$$

This prediction is in good agreement with the measured wavelength of mode A. In a recent experimental study of elliptic instability in a vortex pair (Leweke and Williamson, 1998), the relation between the vortex

core size and the different length scales of the perturbations was determined through precise measurements. Although the vortex pair corresponds to a low-strain elliptic flow, application of these results to the cylinder wake (Williamson, 1996b) yields an estimate for λ_A identical to the one in Equation (4).

The effect of viscosity on the growth rate of the elliptic instability has also been evaluated by Landman and Saffman (1987). Their result for the total growth rate σ can be written as

$$\sigma = \sigma_i - \nu\left(\frac{2\pi}{\lambda}\right)^2 \frac{1-\beta\cos^2\theta}{(1-\beta)\cos^2\theta}. \tag{5}$$

This can be used to obtain an estimate of the growth rate of the mode A instability in the cylinder wake and of its relation to the characteristic time of the periodic base flow.

In fact, the flow conditions in the primary vortices change as the latter are convected away from the near wake. Nevertheless, Figure 8a shows that the flow in the core of a given vortex remains elliptical for at least one shedding period $T = D/US$, where S is the Strouhal number, *i.e.* the non-dimensional shedding frequency. With Equation (2) and $S \approx 0.2$ for the two-dimensional wake at Re = 200 (Barkley and Henderson, 1996), this leads to

$$\sigma T = \frac{1}{S}\left[f(\beta)\left(\varepsilon\frac{D}{U}\right) - \frac{4\pi^2}{(\lambda/D)^2\mathrm{Re}}\frac{1-\beta\cos^2\theta}{(1-\beta)\cos^2\theta}\right] \approx 1.7. \tag{6}$$

The numerical value was obtained with Re = 200, λ/D = 3, and a typical value of the strain, $\varepsilon S/U$ = 0.9, from the DNS data. This result shows that the perturbation developing in a near-wake vortex core can grow by a factor $\exp(\sigma T)$ of more than 5 while instability conditions are favourable. Considering the feedback mechanism discussed in section 2, whereby the initial amplitude of the perturbation grows from one vortex to the next until vortex loops are formed, this growth is sufficient to trigger ultimately the appearance of the non-linear mode A vortex shedding observed in experiments. It is important to notice that the growth rate considered here concerns perturbations inside *one given vortex* as it travels downstream. The growth rates obtained by the Floquet stability analysis of Barkley and Henderson (1996), which are significantly lower, concern the flow *as a whole*. They give a measure of how much a given vortex is more perturbed than its predecessor, and therefore describe primarily the feedback mechanism.

5. Hyperbolic instability and mode B

The link between the theories on the instability of hyperbolic flows and the particular flow encountered in the cylinder wake is somewhat more difficult than for the elliptic instability case. The main reason for this lies in the fact that no general information is available about the features of the most unstable perturbations in a *finite* region of hyperbolic flow. In particular, the spanwise wavelength of the instability cannot be deduced from the cross-sectional size, *i.e.* the thickness, of the hyperbolic shear layer. It seems to depend strongly on the large-scale features of the surrounding flow. Nevertheless, hyperbolic instability has frequently been associated with braid instabilities in other shear flows, like mixing layers (*see*, e.g. Klaassen and Peltier, 1991), Stuart vortices, or Taylor-Green cells (*see* the discussion in Leblanc and Cambon, 1998).

According to Figure 5, the braid shear layer has a thickness $\delta_{\mathrm{braid}} \approx D/4$ for Reynolds numbers in the transition regime. This is confirmed by more precise experimental measurements of the shear layer vorticity

thickness made at a downstream position of one cylinder diameter (Williamson, 1988, unpublished results), which give basically the same result. With the wavelength of mode B given as $\lambda_B = D$, this yields

$$\lambda \approx 4\delta_{\text{braid}}. \tag{7}$$

Although to date there exists no theoretical study of the instability of a strained shear layer which could predict this result, it is nevertheless consistent with the observations made for braid (hyperbolic) instabilities in other flows, as discussed in Williamson (1996b).

One quantitative estimate from hyperbolic instability theory can be made for the cylinder wake; it concerns the growth rate. According to Lagnado *et al.* (1984), the viscous total growth rate σ of the most unstable perturbation is given by

$$\sigma = \sigma_i - \nu\left(\frac{2\pi}{\lambda}\right)^2, \tag{8}$$

where, again, λ is the axial perturbation wavelength. Due to the time dependence of the base flow, it is again useful to evaluate the growth of the instability during the characteristic period T of the flow (*see* section 5). Using Equation (2) and wake units, one obtains

$$\sigma T = \frac{1}{S}\left[\sqrt{1-\beta^{-2}}\left(\varepsilon\frac{D}{U}\right) - \frac{4\pi^2}{(\lambda/D)^2\text{Re}}\right] \approx 7.7, \tag{9}$$

where the experimentally observed wavelength $\lambda = \lambda_B \approx D$ and the estimates $\beta \approx 1.8$ and $\varepsilon D/U \approx 2.1$ from the DNS data for the braid shear layer were used. The high numerical value shows that, even if a given shear layer, like the one depicted in Figures 6 and 8b exists only for a fraction of one shedding cycle, the instability has enough time to reach a significant amplitude during its lifetime.

A final point concerns the small-scale streamwise vortices observed in mode B. The formation of these secondary vortices can be related to the hyperbolic instability by considering the amplification of vorticity perturbations through stretching in the extensional direction of the strain discussed by Lagnado *et al.* (1984) and Leblanc and Godeferd (1998). Similar vortex structures were also found in the recent experiments on hyperbolic flow by Couder (1997). In the braid shear layers of the cylinder wake, the stretching direction of the strain is almost aligned with the layer (see *Fig.* 6). It therefore seems that the observed streamwise vortices can indeed be considered as a consequence of a hyperbolic instability of the braid region.

6. Conclusions

In this paper, we have used results from several different studies in order to explain the physical origin of the instabilities leading to the two distinct modes of three-dimensional vortex shedding observed in the transition regime of the wake of a circular cylinder.

Mode A, which is visible in the Reynolds number range 190-240, is associated with a deformation of the primary vortices and the formation of vortex loops facing upstream. Its spanwise wavelength varies between 3 and 4 cylinder diameters and decreases slightly with Reynolds number. The streamwise vorticity pattern of this large-scale mode exhibits an out-of-phase symmetry between succesive half-cycles of vortex shedding.

Mode B, observed for Re > 240, involves the inception of small-scale streamwise vortex pairs with a spanwise spacing of about one cylinder diameter, which is roughly independent of Reynolds number. These secondary

vortices show an in-phase symmetry between one half-cycle and the next. The symmetries of the two modes can be understood by considering the effect of the feedback between successive primary vortices and the influence of the recirculation region behind the cylinder.

An analysis of the two-dimensional base flow in the transition regime, using results from direct numerical simulations, pointed out the two main structures of the wake: the large-scale primary vortex cores, and the braid shear layers between the vortices, which have a much smaller spatial scale. In the near wake, these regions contain two different basic types of flow: elliptic flow in the cores and hyperbolic flow in the braids. Both types are known to be three-dimensionally unstable. We therefore suggest that the wake transition mode A is a consequence of an elliptic instability of the primary vortex cores in the near wake and scales on the diameter of the cores, whereas mode B is due to a hyperbolic instability of the braid shear layer and scales on the thickness of this layer.

For mode A, comparisons between elliptic instability theory and observations in the wake concerning the spatial structure, wavelength, and growth rate of the perturbations, lend support to the suggestion of an elliptic instability. Concerning mode B, no equivalent predictions from the theory of hyperbolic instability applicable to the cylinder wake is available so far. However, the presence of stretched secondary vortices and the estimated growth rate of the observed perturbations are consistent with the existence of a hyperbolic instability of the braid.

Results from Barkely and Henderson (1996) in their precise Floquet linear stability analysis of the "whole wake", show that the contours of perturbation velocity intensity are centred on the vortex cores for mode A, and on the braid regions for mode B (see their Figure 11 and discussion on page 237). This result is clearly consistent with the ideas here, although as very recently pointed out by Ron Henderson (private communication, June 1998), their Figure 11, which shows these contour levels, is only "qualitative". On the other hand, their Figure 10 shows streamwise and spanwise perturbation vorticity for mode A which, in the near wake region, is evidently not centred on the elliptic vortex core regions. As stated by Henderson (private communication, June 1998); their Figure 10 would appear to "rule out" elliptic instability as the basic mechanism generating mode A instability. These and other such comparisons must of course be made, with an understanding of the relationship between the present type of analysis and the Floquet linear stability analysis, and with experimental results taken into account.

We wish to thank A. Lifschitz and S. Leblanc for helpful discussions, as well as one of the referees for clarifying the issue of mode symmetries. The second author is particularly indebted to J. Lasheras for making clear the link between his discovery (with E. Meiburg) of the two possible symmetries in general wake flows, with those symmetries recently deduced in the bluff body wake. The support from the Ocean Engineering Division of the Office of Naval Research, monitored by Tom Swean (ONR Contracts No. N00014-94-1-1197 and N00014-95-1-0332), and from NATO (Grant No. CRG 970259), is gratefully acknowledged.

REFERENCES

BARKLEY D., HENDERSON R. D., 1996, Three-dimensional Floquet stability analysis of the wake of a circular cylinder, *J. Fluid Mech.*, **322**, 215.

BAYLY B. J., 1986, Three-dimensional instability of elliptical flow, *Phys. Rev. Lett.*, **57**, 2160.

BREDE M., ECKELMANN H., ROCKWELL D., 1996, On secondary vortices in the cylinder wake, *Phys. Fluids*, **8**, 2117.

COUDER Y., 1997, The formation of the vorticity filaments; experiments on the interaction of vorticity and strain, *Proc. Euromech Colloquium 364: "Dynamics and Statistics of Concentrated Vortices in Turbulent Flows"*, Carry-le-Rouet, France, p. 23.

ELOY C., LE DIZÈS S., 1998, Instability of the Burger's and Lamb-Oseen vortices in a strain field, submitted to *J. Fluid Mech.*

GERRARD J. H., 1978, The wakes of cylindrical bluff bodies at low Reynolds number, *Phil. Trans. R. Soc. Lond.* A, **288**, 351.

HAMA F. R., 1957, Three-dimensional vortex pattern behind a circular cylinder, *J. Aero. Sci.*, **24**, 156.

JULIEN S., LASHERAS J. C., CHOMAZ J.-M., 1997, Measurements of the onset and growth rate of three-dimensional instabilities in free shear flows, *Bull. Am. Phys. Soc.*, **42**, 2191.

KARNIADAKIS G. E., TRIANTAFYLLOU G. S., 1992, Three-dimensional dynamics and transition to turbulence in the wake of bluff objects, *J. Fluid Mech.*, **238**, 1.

KLAASSEN G. P., PELTIER W. R., 1991, The influence of stratification on secondary instability in free shear layers, *J. Fluid Mech.*, **227**, 71.

LAGNADO R. R., PHAN-THIEN N., LEAL L. G., 1984, The stability of two-dimensional linear flows, *Phys. Fluids*, **27**, 1094.

LANDMAN M. J., SAFFMAN P. G., 1987, The three-dimensional instability of strained vortices in a viscous fluid, *Phys. Fluids*, **30**, 2339.

LASHERAS J. C., MEIBURG E., 1990, Three-dimensional vorticity modes in the wake of a flat plate, *Phys. Fluids* A, **2**, 371.

LEBLANC S., CAMBON C., 1998, Effects of the Coriolis force on the stability of Stuart's vortices, *J. Fluid Mech.*, **356**, 353.

LEBLANC S., GODEFERD F. S., 1998, Hyperbolic instability and formation of ribs in Taylor–Green cells, *Phys. Fluids*, submitted.

LEWEKE T., PROVANSAL M., 1995, The flow behind rings: bluff body wakes without end effects, *J. Fluid Mech.*, **288**, 265.

LEWEKE T., WILLIAMSON C. H. K., 1998, Cooperative elliptic instability of a vortex pair, *J. Fluid Mech.*, **360**, 85.

LIFSCHITZ A., HAMEIRI E., 1991, Local stability conditions in fluid dynamics, *Phys. Fluids* A, **3**, 2644.

MANSY H., YANG P., WILLIAMS D. R., 1994, Quantitative measurements of spanwise periodic three-dimensional structures in the wake of a cylinder, *J. Fluid Mech.*, **270**, 277.

MEIBURG E., LASHERAS J. C., 1988, Experimental and numerical investigation of the three-dimensional transition in plane wakes, *J. Fluid Mech.*, **190**, 1.

MITTAL R., BALACHANDAR S., 1995, Generation of streamwise vortical structures in bluff-body wakes, *Phys. Rev. Lett.*, **75**, 1300.

NOACK B. R., ECKELMANN H., 1994, A global stability analysis of the steady and periodic cylinder wake, *J. Fluid Mech.*, **270**, 297.

PERSILLON H., BRAZA M., 1998, Physical analysis of the transition to turbulence in the wake of a circular cylinder by three-dimensional Navier-Stokes simulation, *J. Fluid Mech.*, **365**, 23.

PIERREHUMBERT R. T., 1986, Universal short-wave instability of two-dimensional eddies in an inviscid fluid, *Phys. Rev. Lett.*, **57**, 2157.

THOMPSON M., HOURIGAN K., SHERIDAN J., 1996, Three-dimensional instabilities in the wake of a circular cylinder, *Exp. Therm. Fluid Sci.*, **12**, 190.

WALEFFE F., 1990, On the three-dimensional instability of strained vortices, *Phys. Fluids* A, **2**, 76.

WILLIAMSON C. H. K., 1988, The existence of two stages in the transition to three-dimensionality of a cylinder wake, *Phys. Fluids*, **31**, 3165.

WILLIAMSON C. H. K., 1996a, Vortex dynamics in the cylinder wake, *Annu. Rev. Fluid Mech.*, **28**, 477.

WILLIAMSON C. H. K., 1996b, Three-dimensional wake transition, *J. Fluid Mech.*, **328**, 345.

ZHANG H.-Q., FEY U., NOACK B. R., KÖNIG M., ECKELMANN H., 1995, On the transition of the cylinder wake, *Phys. Fluids*, **7**, 779.

(Received 23 December 1997,
revised 5 March 1998,
accepted 6 March 1998)